American Mineralogist, Volume 96, pages 1703–1717, 2011

Ammonium vermiculite in schists from the Betic Cordillera (Spain)

M.D. Ruiz Cruz*

Facultad de Ciencias, Campus de Teatinos, 29071 Málaga, Spain

Abstract

NH_4-bearing phases from pre-Permian schists of the Internal Zones of the Betic Cordillera (Spain) have been characterized by X-ray diffraction, differential thermal analysis and thermogravimetry, infrared spectroscopy, and transmission-analytical electron microscopy. The content and distribution of NH_4 in these phases have been estimated by combining elemental analysis of N with mineral quantification based on X-ray diffraction, whole-rock composition, and electron microprobe data. The obtained results indicate that the NH_4 content in vermiculite ranges between ~0.5 and ~1.0 (wt%), leading to terms with NH_4 > K in the interlayer. The NH_4 content is <0.30 (wt%) in biotite from underlying schists. Muscovite shows very low NH_4 contents (0.04 wt%) through the complete sequence. We interpret that, initially contained in low-grade dioctahedral mica, NH_4 was incorporated in the structure of the trioctahedral phases formed at increasing metamorphic conditions. The entry of NH_4 in the interlayer was favored in chlorite:vermiculite mixed-layered structures and transitional phases with vacancies in the A site (vermiculite) and weak cohesion between layers. NH_4 appears to favor the formation of intermediate phases instead the direct transformation of chlorite to biotite.

Keywords: Ammonium mica, biotite, Betic Cordillera, Spain, muscovite, suhailite, vermiculite

Introduction

The terms "high-temperature vermiculite" or "metamorphic vermiculite" were proposed by Velde (1978) for a yellow-to-brown phyllosilicate present in metamorphic sequences just below the biotite zone. Metamorphic vermiculite is characterized by high birefringence, chemical composition similar to chlorite but containing K and Ca, and thermal behavior similar to vermiculite. Later studies of phases interpreted as metamorphic vermiculite revealed, however, that they might include either muscovite-chlorite intergrowths (Franceschelli et al. 1986; Mellini et al. 1991) or mixed-layered structures (Maresch et al. 1985; Ruiz Cruz 1999, 2001) in addition to discrete vermiculite (Ruiz Cruz 1999). These phases have been interpreted in some cases as formed from chlorite during prograde metamorphism (e.g., Kerrick and Cotton 1971; Velde 1978; Maresch et al. 1985; Ruiz Cruz 1999, 2001), although there is also evidence of the formation of similar phases during weathering or retrograde processes affecting both chlorite and biotite (Johnson 1964; Brown 1967; Proust 1982; Proust et al. 1986).

Formation of vermiculite from chlorite during prograde metamorphism is well documented in pre-Permian units from the Maláguide complex (Internal Zones of the Betic Cordillera, Spain). This metamorphic sequence contains a series of phases chemically and structurally "intermediate" between chlorite and biotite. According to interpretations of X-ray data and transmission electron microscopy studies, these phases, named as a whole vermiculite, include muscovite:chlorite and chlorite:vermiculite mixed-layer minerals as well as intermediate steps in the chlorite-to-biotite transformation (Ruiz Cruz and Nieto 2006). This sequence appears to demonstrate a continuous transitional phase transformation in the rocks studied herein.

Due to the discovery of the presence of ammonium-rich di- and trioctahedral micas (tobelite and suhailite, respectively) in the lowest strata (Paleozoic or older) of the Internal Zone complexes (Ruiz Cruz and Sanz de Galdeano 2008, 2009a, 2009b), we have performed a systematic analysis of the pre-Permian units to investigate for the possible presence of NH_4 in phyllosilicates in these metamorphic units.

NH_4 is not detected by the routine analytical methods applied in metamorphic petrology and is therefore generally overlooked in such studies. Other methods need to be included in the analyses to estimate NH_4 in phyllosilicates, such as elemental analysis of nitrogen (Schroeder and Ingall 1994), infrared spectroscopy (Busigby et al. 2003), and data derived from the basal spacing of the mica minerals (Drits et al. 1997, 2005). This study focuses on the characterization of NH_4-bearing vermiculite, present in units intermediate between the Maláguide and the Alpujárride complexes, with the aim of interpreting its relations with chlorite from overlying schists and with biotite present in the underlying schists, the crystal-chemical factors that control the entry of NH_4 in the interlayer, and its possible geochemical significance in influencing mineral transformation reactions during prograde metamorphism.

Geological setting

The Betic cordillera (SE Spain) makes up part of the peri-Mediterranean Alpine orogenic system (Fig. 1). This cordillera has been traditionally divided into an External Zone, consisting of Triassic to Middle Miocene sedimentary rocks, and an Internal Zone, composed mainly of Paleozoic and Triassic metamorphic rocks.

The Internal Zone is generally subdivided into three nappe complexes named, from top to bottom: the Maláguide, the Alpujárride, and the Nevado-Filábride. Generally, Maláguide and Alpujárride Permo-Triassic units are easily distinguished on the basis of their different lithologies and metamorphic grade.

* E-mail: mdruiz@uma.es

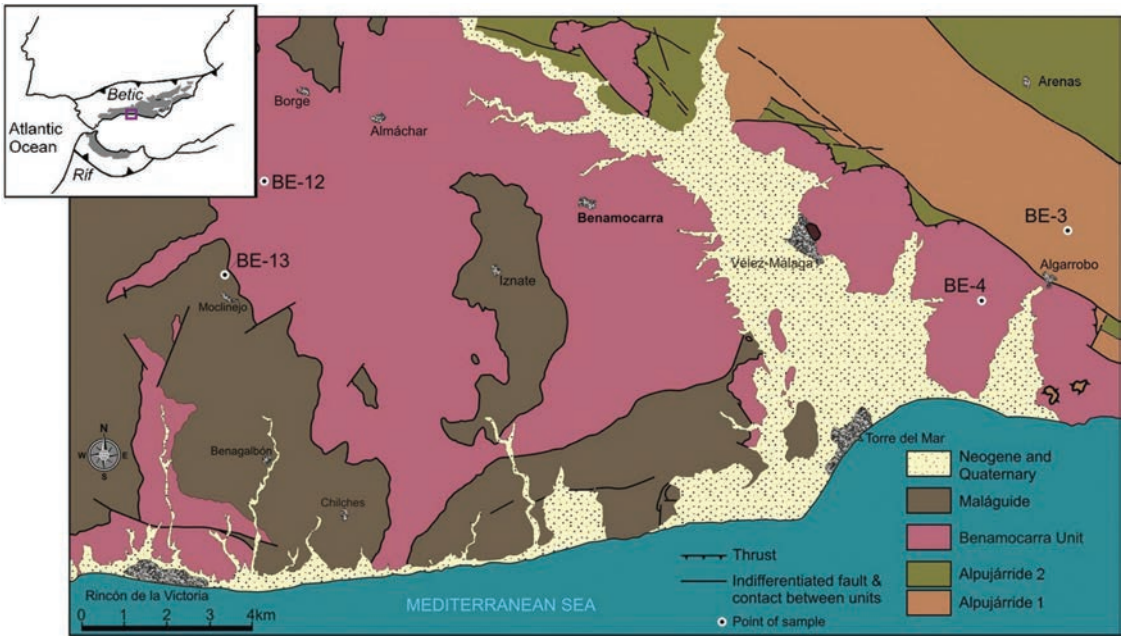

Figure 1. Simplified geologic map of the studied area. The positions of the lowest unit of the Maláguide Complex, the Benamocarra unit, and two superimposed units (Alpujárride 1 and Alpujárride 2) of the Alpujárride Complex as well as sample locations are shown. Inset: Westernmost part of the Mediterranean Alpine belt. The Betic-Rif Internal Zone is shown in gray.

Nevertheless, transitional zones with intermediate lithologies and metamorphism have been identified in several areas of the Cordillera and are known as "intermediate units" (Sanz de Galdeano et al. 2001). Moreover, distinction between the pre-Permian formations of both complexes is difficult in some zones. This occurs for example near Málaga, where an intermediate unit (Benamocarra) has been defined (Estévez and Chamón 1972; Elorza and García-Dueñas 1981).

Both the Alpujárride and the Maláguide complexes show plurifacial metamorphism. In the Alpujárride complex, a Hercynian event deduced from zircon dating (e.g., Zeck and Williams 2001) was followed, according to previous interpretations, by two main Alpine episodes: A first high-pressure/low-temperature (HP/LT) event associated with the early crustal-thickening stage and a low-pressure/high-temperature (LP-HT) event, characterizing isothermal decompression (e.g., Goffé et al. 1989; Tubía et al. 1992; García-Casco and Torres-Roldán 1996; Azañón and Goffé 1997). The Maláguide complex has undergone Alpine metamorphism ranging from relatively low-temperature diagenetic conditions to the highest temperature anchizone type conditions in the Permo-Triassic red beds (Ruiz Cruz and Rodríguez Jiménez 2002). The Paleozoic series preserve clear Hercynian orogenic features characterized by greenschist facies metamorphism (Ruiz Cruz and Sanz de Galdeano 2010).

Sampling and methodology

Sampling was conducted in the area shown in Figure 1, in the Málaga province of Southern Spain. From the numerous samples studied, which will be used in a subsequent paper (Ruiz Cruz and Sanz de Galdeano in prep.) devoted to the analysis of the metamorphic evolution, we have selected four samples for detailed crystal-chemical study. These samples are representative of the lowest Maláguide Complex unit, the Benamocarra unit and the pre-Triassic formations of the Alpujárride complex. Samples were analyzed by petrography, X-ray diffraction (XRD), Fourier transform infrared spectroscopy (FTIR), and differential thermal analysis-thermogravimetry (DTA-TG). Carbon and N determinations were carried out by elemental analyses. The chemical characterization was conducted by electron microprobe analysis (EMPA) and analytical electron microscopy (AEM).

XRD patterns were recorded using a Philips X'Pert PRO MPD (University of Málaga), with Cu$K\alpha$ radiation and Ge monochromator, operating at 40 mA and 40 kV, with 0.01 °θ step size and variable counting time. Randomly oriented samples were used to determine the quantitative mineral composition, using the Rietveld-based X'Pert High Score Software package (Philips) and the PDF2-2003 database (International Center for Diffraction Data). Patterns from natural and Mg-saturated (air-dried and glycolated) oriented samples were obtained for mineral structure characterization of the phyllosilicates. FTIR spectra were recorded in KBr pellets (2 wt% samples) using a Nicolet spectrometer (20SXB) with a DTGS detector, in the range 4000–400 cm^{-1} (Málaga University). Resolution was 2 cm^{-1}. DTA-TG curves were performed with a Netzsch STA 409 PE apparatus using platinum/rhodium thermocouples and platinum crucibles. The following experimental conditions were used: sample weight = 15 mg, temperature range = 20–1020 °C, heating rate = 10°/min; reference: Al_2O_3; static air atmosphere.

EMPA data were obtained with a Cameca SX100 microprobe in the Centro de Instrumentación Científica (CIC, Granada University) with an accelerating voltage of 20 kV, a 20 nA beam current, and a beam diameter of 5 μm. The data were reduced

using the X-PHI correction. Standards were albite (Na), periclase (Mg), synthetic SiO_2 (Si), Al_2O_3 (Al), TiO_2 (Ti), Fe_2O_3 (Fe), Cr_2O_3 (Cr), NiO (Ni), $MnTiO_3$ (Mn), sanidine (K), and diopside (Ca).

Samples were ion thinned for transmission-analytical electron microscopy (TEM-AEM) study. This study was carried out with a Philips CM-20 transmission electron microscope (TEM) operated at 200 kV and fitted with a scanning transmission device and solid-state detector for energy-dispersive analysis (CIC, Universidad de Granada). Microanalyses were obtained in STEM mode. Quantitative determinations used the thin-film approximation of Cliff and Lorimer (1975). Standards were: albite (Na); muscovite and annite (K); albite, spessartine, and muscovite (Al); forsterite and annite (Mg and Fe); spessartine (Mn); and titanite (Ca and Ti).

The analyses for N and C were performed with an 1108 (Carlo Erba) CHN analyzer (University of La Coruña). Analysis conditions were: oxidation temperature = 1020 °C; reduction temperature = 650 °C; $P(O_2)$ = 100 kPa. The standard used was sulfanilamide (BBOT). The detection limit is 0.001 wt%. Replicate analyses indicate that the error in N determination is <0.005%.

The abbreviations of minerals of Whitney and Evans (2010) have been used in the text, tables, and figures, with some additions indicated in the captions of the figures or tables. The abbreviation "Ms" includes muscovite and possible phengite.

Petrography

The samples described here include one very fine-grained andalusite schist from the Maláguide complex (sample BE-13), two fine-grained andalusite-garnet schists from the Benamocarra unit (samples BE-12 and BE-4), and one andalusite-sillimanite-staurolite schist from the Alpujárride complex (BE-3), which are representative of increasing metamorphic grade (Table 1).

The Maláguide sample shows the assemblage Qz+Pl+Ms+Chl+Vrm+Cld+And; since chlorite is a major constituent, is referred to as chlorite schist for simplification. The chlorite schist is fine grained, with the main regional schistosity (S_p) defined by alternating quartz+plagioclase and phyllosilicates-rich bands (Fig. 2a). Chlorite, with only subordinate vermiculite, is the main trioctahedral phyllosilicate according to the optical study and the XRD patterns. Vermiculite schists, which exhibit a gaudy yellow color in hand-specimen, have textures characterized by alternating muscovite-rich bands and quartz-rich areas, defining S_p.

The vermiculite schists lack chlorite; vermiculite is the dominant mafic phyllosilicate. Although fine grained, these samples contain large garnet porphyroblasts (Fig. 2b). Coarser-grained vermiculite, appropriate for optical and chemical studies, is found in pressure shadows. The vermiculite has a yellow-to-brown color and pleochroism and second-order birefringence (Figs. 2b and 2c), optical properties that agree with previous descriptions of metamorphic vermiculite (e.g., Black 1975; Velde 1978; Nicot 1981; Ruiz Cruz and Nieto 2006). Samples from the Benamocarra unit are characterized by the assemblage Qz+Pl+Ms+Vrm±Chl-Vrm ML±Cld+And+Grt and are referred to as vermiculite schists.

The schist from the Alpujárride complex is characterized by the assemblage Qz+Pl+Ms+Bt+Sil+And+St+Grt, with minor amounts of Vrm, and is referred to as biotite schist. Biotite is the main trioctahedral phyllosilicate observed in the biotite schist from the Alpujárride complex. Two optically and texturally different biotite populations are evident: red biotite, unoriented with respect to the main schistosity and partially replaced by sillimanite; and golden biotite, sub-parallel to S_p (Fig. 2d).

FTIR, DTA, and XRD data

FTIR spectra in the zone of the OH-stretching vibrations are strongly influenced by the presence of abundant muscovite, which shows the main band at 3625 cm^{-1}. Differences between vermiculite- and biotite-bearing samples are reflected in the presence of a 3592 cm^{-1} band in the spectrum of sample BE-3, which is ascribed to the presence of vacancies in the octahedral sheet of the biotite structure (Farmer 1974), and the intensity of the broad band between 3200 and 3500 cm^{-1}, due to the O-H bond stretching vibrations of water, which is higher in the spectrum of sample BE-12 (Fig. 3a). The presence of NH_4 was confirmed in all samples by a characteristic band in the zone of the N-H vibrations (Chourabi and Fripiat 1981; Busigby et al. 2003); the highest intensities are present in the Benamocarra samples. The N-H band shows maxima at 1425 and 1455 cm^{-1} (Fig. 3b). Moreover, the spectra show small bands at ~1540 cm^{-1}. This value is similar to that found in some ammonium halides, and could be interpreted as due to shortening of the H-bridges in NH_4 coordinated to water molecules (Russell and White 1988). Furthermore, the biotite schist shows a sharp graphite band at 1382 cm^{-1} (Fig. 3).

The DTA and TG curves of samples BE-12 and BE-3 show more evident differences (Fig. 4). The dehydration peak maximum is at 100 °C in the case of sample BE-3, and represents loss of either adsorbed water or water contained in vermiculite. Water is lost in several stages in sample BE-12. Moreover, the intensity of the endothermic effects, as well as the associated mass loss (TG curves), were very different as sample BE-12 is more hydrated than sample BE-3, which corroborates the FTIR results. The weak endothermic effect at 318 °C in the DTA curve of sample BE-12 probably corresponds to the thermal decomposition of NH_4^+, as observed in NH_4-smectite (Gautier et al. 2010). Moreover, whereas sample BE-12 shows a single dehydroxylation endothermic peak (at 500°), which must include mixed-layers and muscovite dehydroxylation, sample BE-3 shows two overlapping endothermic effects, which are difficult to interpret since the sample contains two biotite populations

Table 1. Location, lithology, and mineralogy of the samples studied

Samples	Complex	Location	Classification	Mineralogy
BE-13	Maláguide	N36°46′36.7″-W04°15′11.7″	And-Chl schist	Qz+Pl+Ms+Chl+Vrm+Cld+And
BE-12	Benamocarra	N36°47′50.2″-W04°14′0.3″	And-Grt Vrm schist	Qz+Pl+Ms+Vrm+ML+Grt+Cld+And
BE-4	Benamocarra	N36°46′3.6″-W04°3′27.6″	Grt-Vrm schist	Qz+Pl+Ms+Vrm+Grt
BE-3	Alpujárride	N36°47′2.5″-W04°01′56.7″	And-St-Bt schist	Qz+Pl+Ms+Bt+(Vrm)+And+St+(Sil)+Grt+Kln

Note: ML: Chlorite-vermiculite mixed-layers.

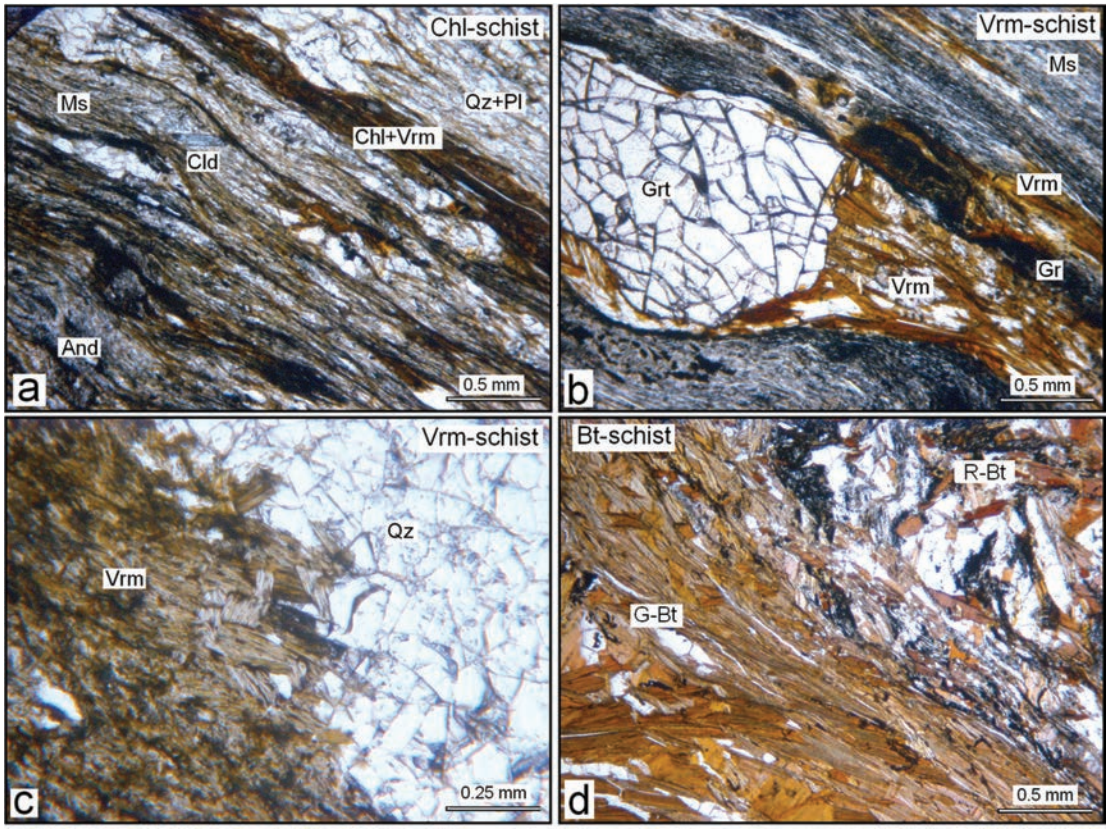

Figure 2. Photomicrographs of selected schists. (**a**) Maláguide andalusite-chlorite schist with the assemblage Qz+Pl+Ms+Chl+Vrm+Cld+And (sample BE-13). Fine intergrowths of chlorite and vermiculite show a brownish color. (**b**) Benamocarra andalusite-garnet-vermiculite schist with the assemblage Qz+Pl+Ms+ML+Vrm+And+Grt (sample BE-12). Mixed-layers (ML) chlorite-vermiculite and vermiculite follow S_p and are present in the pressure shadows. (**c**) Benamocarra garnet-vermiculite schist with the assemblage Qz+Pl+Ms+Vrm+And+Grt (sample BE-4). (**d**) Alpujárride sillimanite-andalusite-staurolite-biotite schist with the assemblage Qz+Pl+Ms+Bt+St+Sil+Grt+And (sample BE-3). Two generations of biotite appear in this sample: early red biotite (R-Bt), partially transformed into sillimanite, and later golden biotite (G-Bt), which follows S_p.

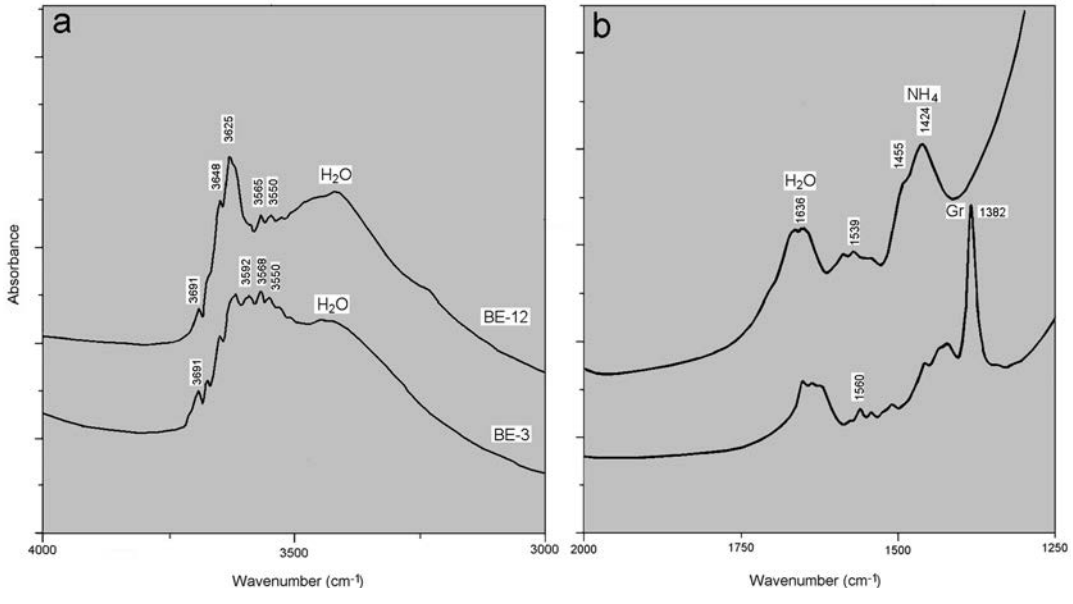

Figure 3. FTIR spectra of samples BE-12 (containing ML+Vrm) and sample BE-3 (containing Bt) in the zones 4000–3000 cm^{-1} (**a**) and 2000–1250 cm^{-1} (**b**). See text for explanation.

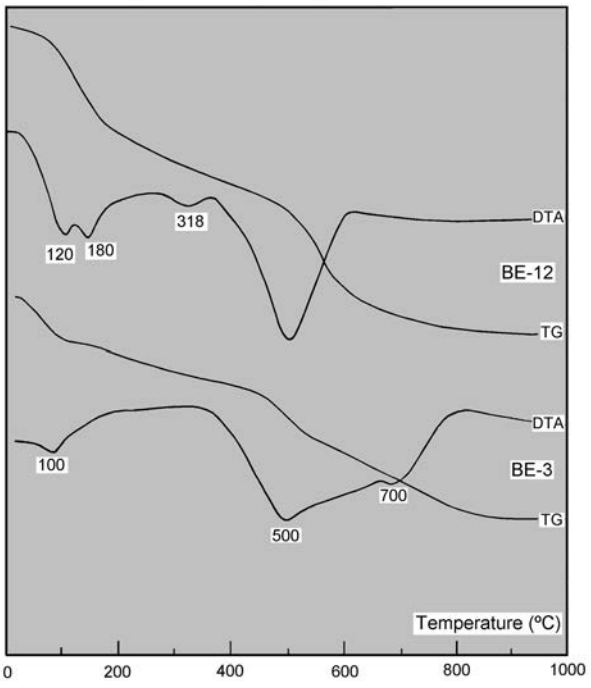

FIGURE 4. TG and DTA curves of samples BE-12 and BE-3. See text for explanation.

and minor vermiculite in addition to muscovite.

XRD patterns obtained from natural samples (Fig. 5a) suggest the prevalence of chlorite in sample BE-13. Vermiculite is dominant in samples BE-12 and BE-4, whereas biotite is dominant in sample BE-3. Nevertheless, sample BE-13 also contains vermiculite, whereas sample BE-12 contains the assemblage chlorite:vermiculite mixed-layer + vermiculite. Sample BE-4 contains only vermiculite. Chlorite and vermiculite are differentiated in the XRD patterns obtained from air-dried samples by the width of the basal reflections (notably broader in vermiculite) and the relative intensity of the 001 and 002 reflections. The presence of vermiculite and chlorite:vermiculite mixed-layers was tested by heating the samples at increasing temperatures, and by examining patterns obtained after Mg-saturation and glycolation. Heating caused the progressive contraction of the 14 Å vermiculite or mixed-layer reflection. In samples containing dominant chlorite, the thermal treatment led to an increase in the intensity of the 001 reflection and the decrease of the 002 reflection. In samples containing vermiculite and mixed-layer phases, contraction after heating to 500 °C produced discrete reflections of mixed-layers at ~12 and ~8 Å, whereas vermiculite contracted to ~10 Å. In samples containing only vermiculite, the 10 Å reflection notably increased in intensity after heating (Fig. 5b).

XRD patterns of air-dried Mg-saturated samples (Fig. 5c) show scarce differences (a slight contraction of the basal spacing from ~14.3 to 14.0 Å in vermiculite) with those obtained from natural samples, except in the case of sample BE-3, in which Mg-saturation originates a broad band between 10 and 12 Å, and a small reflection at 14 Å. The patterns obtained after glycolation of the Mg-saturated samples (Fig. 5d) also show slight modifications (very slight expansion from 14 to 14.12 Å) relative to those obtained from the air-dried Mg-saturated samples, except in the case of the sample BE-3, in which the wide band observed between 10 and 12 Å is better resolved (and centered at 11.1 Å), suggesting the presence of discrete vermiculite (14 Å) and mixed-layers biotite-vermiculite (11.1 Å).

Careful examination of the basal spacing of muscovite (based on the position of the 005 reflection, indices corresponding to the one-layer polytype) indicates that the transition from chlorite to vermiculite schist is accompanied by a shift of the 005 reflection of muscovite from 1.994 to 1.999 Å (which correspond to a basal spacing of 9.99 Å). Using the linear regression deduced by Drits et al. (1997) (W_{NH_4} = 13.93, d_{005} – 27.79), very low values of W_{NH_4} (near 0.00 wt%) have been estimated for muscovite in the chlorite schist sample, and values of 0.056 wt% in the vermiculite schist samples. These values are considered as approximations, since the regression was derived from a diagenetic dioctahedral NH_4-bearing illite sample set. The XRD patterns of schists containing chlorite+vermiculite, mixed-layers+vermiculite or only vermiculite were used for characterizing the NH_4-bearing phases (Table 2). Chlorite shows a mean basal spacing of 14.158 Å (σ = 0.033). The average basal spacing of the 1:1 mixed-layer phases is 28.684 Å, with relatively high σ (0.157). Nevertheless, this sample also contains minor amounts of vermiculite and an ordered mixed-layer chlorite:vermiculite mineral with approximately 67% chlorite layers, as indicated by the asymmetry of the main basal reflections (Fig. 5a) and the lattice-fringe images (see below). The average basal spacing for vermiculite, determined in sample BE-12, is 14.283 Å (σ = 0.09) and slightly higher (14.301 Å, σ = 0.049) in sample BE-4.

NH_4 content and distribution in phyllosilicates

Given the fine-grained nature of the phyllosilicates in the samples studied, elemental analysis of N was carried out on whole rock samples. Although some NH_4 could be present in plagioclase (Honma and Itihara 1981), it only represents about 7% of the NH_4 content in mica so we will assume that most NH_4 is contained in phyllosilicates. The values determined are uniform (between 0.046 and 0.082 wt%, Table 3) although N contents up to 0.098 wt% were observed in other vermiculite schists not included in this work. Estimation of the exact amounts of NH_4 in the several types of phyllosilicates coexisting in a given sample is difficult, but some approximations are possible. For example, the FTIR spectra and the XRD data strongly suggest that muscovite in the samples studied here is NH_4-poor, whereas biotite contains NH_4 and highest concentrations of NH_4 appear to be contained within the vermiculite phase (Fig. 3). Estimation of the NH_4 content in the different phyllosilicate populations requires accurate quantification which can be realized by means of a Rietveld-based XRD method, or by using whole-rock compositions and EMPA data in samples only containing muscovite or biotite (not shown in this work). Using such methods, we have deduced the NH_4 content in muscovite from muscovite+chlorite schists. The results obtained using the whole-rock composition and XRD-based methods are very similar (0.035–0.042 wt%). Based on the muscovite and biotite contents estimated from the XRD patterns, and assuming a NH_4 content in muscovite of 0.04 wt%, the determined NH_4 content in biotite from sample BE-3 is 0.28 wt% (Table 3). The XRD-based quantification has, however,

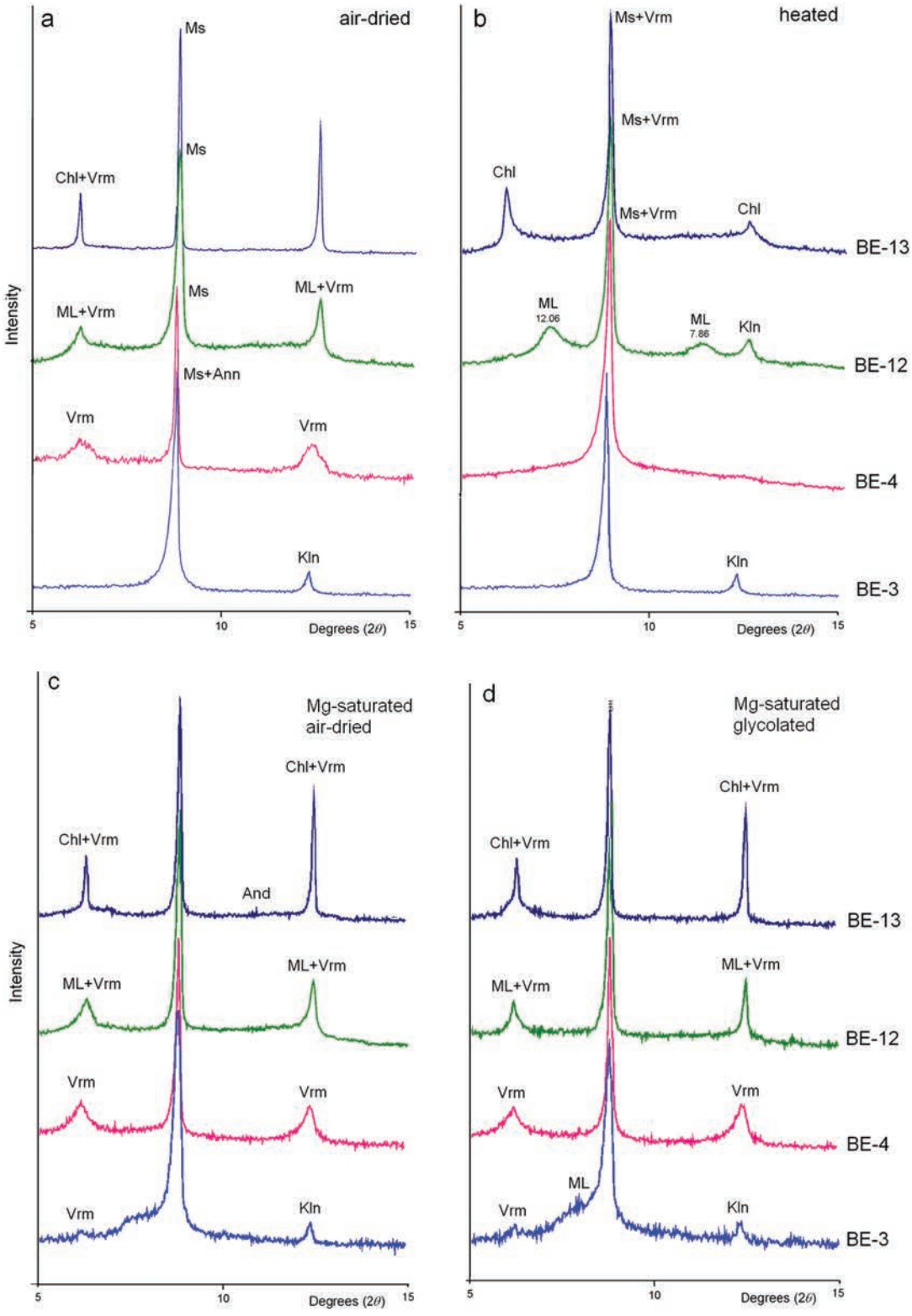

FIGURE 5. The 5–15 (°2θ) zone of the XRD patterns (oriented samples) of the studied schists showing the evolution of the phyllosilicate assemblage with increasing metamorphic grade. (**a**) Air-dried natural samples. (**b**) Natural samples heated to 500 °C. (**c**) Air-dried Mg-saturated samples. (**d**) Glycolated Mg-saturated samples. ML indicates chlorite-vermiculite mixed-layers in sample BE-12 and probable biotite-vermiculite mixed-layers in sample BE-3.

TABLE 2. Main reflections for chlorite, chlorite:vermiculite mixed-layers, and vermiculite

	BE-13 (Chl)		BE-13 (Vrm)		BE-12 (ML)		BE-4 (Vrm)		
hkl	*d* (Å)	*I*	*d* (Å)	*I*	*d* (Å)	*I*	*d* (Å)	*I*	FWHH
001	14.191	*	14.191	*			14.387	56	0.497
002	7.068	*	7.068	*	14.392	86	7.165	81	0.488
003	4.732	30	4.772	33			4.762	41	0.436
004	3.534	100	3.579	*	7.116	100	3.553	100	0.408
005	2.826			12	5.681	10	2.859	63	
006			2.387	6	4.793	28	2.378	38	0.384
007					4.058		2.042	14	
008			1.801	<5	3.589	80			
009					*	*	1.590	9	
00,10					*	*			
00,11					2.614	10			
00,12					2.392	15			
00,13					2.214	10			
00,14					2.056	10			
00,15					1.922	10			
00,16					1.802	5			
00,17									
00,18					1.598	10			
Avg.	14.158		14.283		28.684		14.301		
σ	0.033		0.090		0.157		0.049		

* Reflections overlapping with other phases.

TABLE 3. Nitrogen and carbon contents and estimation of the NH_4 content (wt%) in the various phyllosilicates

Sample	C	N	Ann	Ms	Chl+Vrm+ML*	NH_4(Ms)	NH_4(Vrm)*	NH_4(Ann)
BE-13	0.42	0.061	0	61	6 (Chl+Vrm)	0.04		
BE-12	0.71	0.082	0	58	7 (10) (Vrm+ML)	0.04	1.08 (0.76)	
BE-4	0.71	0.056	0	56	9 (12) (Vrm)	0.04	0.48 (0.36)	
BE-3	0.70	0.046	14	28	4 (Vrm)	0.04	?	0.28

* Values obtained from X-ray quantification and from whole-rock composition (in parentheses).

important restrictions in the case of vermiculite schists, due to lack of data specific to vermiculite and chlorite-vermiculite mixed-layer phases in the database used for the quantification procedure. Because of this limitation, we quantified the aggregate sum of vermiculite+mixed-layer chlorite-vermiculite phases, using the XRD intensity correction factor corresponding to chlorite with a composition similar to chlorite from sample BE-13.

In parallel, calculations of the weight percent fraction of vermiculite+mixed-layer minerals contents were obtained using whole-rock compositions (Table 4) for an independent corroboration of XRD-based estimates. In the latter case, we assumed that K_2O, FeO, and MgO are mainly contained in vermiculite+chlorite-vermiculite mixed-layer aggregate phase and in muscovite, and we have used the average EMPA data for calculating the distribution of these oxides between the two phases. The obtained vermiculite+mixed-layer contents are systematically higher (~20%) when using whole-rock compositions than using XRD estimates. This overestimation from the whole-rock chemistry data is consistent with expectations because there are other FeO and MgO-bearing mineral phases present in the samples (e.g., chloritoid, garnet, and Fe-oxide). The estimated NH_4 contents in trioctahedral phylloslicates, based on the XRD quantification, range from 1.08 wt% in sample BE-12 to 0.48 wt% in sample BE-4 and 0.28 wt% in sample BE-3. Despite the uncertainty inherent in the estimation procedures, these data (Table 3) suggest a trend of decreasing NH_4 contents in minerals and whole-rock samples with increasing metamorphic grade. The observed preferential fractionation of NH_4 into biotite and vermiculite vs. muscovite is in accordance with previous data (e.g., Honma and Itihara 1981; Duit et al. 1986; Boyd and Philippot 1998). It has been speculated in these previous studies that this preference is due to the larger 12-fold site in biotite, which can more easily accommodate the larger NH_4 ion. Data in Table 3 indicate that the NH_4 content in biotite is roughly 0.28 wt% and notably higher in vermiculite (and particularly enriched in the chlorite:vermiculite mixed-layer phase) present in samples with lower metamorphic grade. This NH_4 enrichment cannot be related to higher organic matter contents in vermiculite-bearing samples because the C content is similar in both groups of samples (Table 3). It is speculated that NH_4 enrichment in mixed-layer chlorite-vermiculite phases and vermiculite could reflect the lower metamorphic grade of these samples, or be controlled by crystal-chemical factors.

CHEMICAL DATA

Chemical data for chlorite, mixed-layers chlorite:vermiculite, vermiculite, and biotite (average data) are reported in Table 5. In the analyses of mixed-layers chlorite-vermiculite and vermiculite, the estimated $(NH_4)_2O$ contents have been included. Average chlorite analysis show low Si content (2.58 atoms per formula unit, apfu) and $X_{Mg} = 0.32$ [X_{Mg} = Mg/(Fe+Mg)], corresponding to chamosite (Table 5, analysis 1). Analyses of mixed-layer phases show K_2O contents < 1.5 wt% (Table 5, analysis 2), whereas vermiculite analyses show K_2O contents ranging from 3.0 to 4.0 wt% (Table 5, analysis 3). Mixed-layer formulas calculated on the basis of a 25 oxygen unit cell and accounting for the estimated NH_4 contents, suggest that the vermiculite layers contain NH_4 > K in the interlayer. The average formula of vermiculite shows an interlayer occupancy near the ideal 0.7 apfu. The formula shows an octahedral occupancy >3.0 apfu, suggesting the contribution of minor chlorite in the chemical analyses. As a whole, the evolution from chlorite to chlorite:vermiculite mixed-layers and to vermiculite is characterized by an increase in SiO_2, TiO_2, K_2O, X_{Mg}, and H_2O and by the parallel decrease in Al_2O_3 and FeO+MgO.

The transition from vermiculite to biotite (annite) is sharp and clearly marked by the higher total K_2O content. Analyses of red and golden biotite show some differences, primarily in their Ti and K contents (both higher in red biotite) and in their ^{VI}Al content (higher in golden biotite). Although the amount of NH_4 in golden biotite could not be estimated, the coexistence of golden and red biotite in sample BE-3 and the data in Table 5 (analyses 4 and 5) suggest that the mean NH_4 content estimated for biotite (Table 3) is likely within the golden biotite phase. Indeed, although variations in individual grains were observed,

TABLE 4. XRF data for whole samples

wt%	BE-13	BE-12	BE-4	BE-3
SiO_2	59.11	46.00	54.10	58.27
Al_2O_3	20.91	29.74	22.87	19.87
Fe_2O_3	7.65	6.28	6.60	8.71
MnO	0.11	0.09	0.05	0.08
MgO	1.58	1.64	3.79	2.32
CaO	0.65	1.29	0.22	0.87
Na_2O	0.60	1.22	0.06	0.83
K_2O	3.54	6.22	4.99	4.03
TiO_2	1.02	1.53	1.04	1.27
P_2O_5	0.14	0.17	0.14	0.17
LOI	4.15	5.50	5.77	3.15
Total	99.46	99.67	99.62	99.58

TABLE 5. Chemical data for trioctahedral phyllosilicates

	Avg. Chl (BE-13)		Avg. ML (BE-12)		Avg. Vrm (BE-4)		Red Ann		Golden Ann		Suh
	1 (n=3)	σ	2 (n=14)	σ	3 (n=10)	σ	4 (n=13)	σ	5 (n=8)	σ	6
SiO_2	23.20	0.53	27.89	1.49	30.02	2.21	34.73	1.48	35.88	2.11	35.77
TiO_2	0.09	0.02	0.24	0.16	1.03	0.52	2.92	0.67	1.94	0.09	3.97
Al_2O_3	21.10	0.35	18.97	1.30	18.21	0.49	19.71	0.91	20.96	1.49	19.93
Cr_2O_3	0.05	0.03	0.07	0.06	0.09	0.06	0.06	0.08	0.03	0.01	0.00
FeO	33.75	0.45	26.13	0.86	18.26	4.42	21.69	0.63	20.89	1.29	21.27
MnO	0.40	0.10	0.13	0.08	0.07	0.10	0.09	0.02	0.14	0.03	0.18
MgO	9.01	0.23	7.28	0.62	8.09	0.71	6.89	0.72	7.45	0.93	6.42
CaO	0.12	0.09	0.50	0.21	0.33	0.06	0.22	0.09	0.52	0.06	0.62
Na_2O	0.12	0.02	0.08	0.12	0.46	0.22	0.11	0.03	0.12	0.02	0.48
K_2O	0.09	0.06	1.21	0.62	3.36	1.27	8.36	0.67	5.70	0.59	3.66
$(NH_4)_2O$*			1.70		0.81						2.60
Total	87.92	1.16	84.19	3.31	80.73	0.74	94.92	3.65	94.17	5.57	95.60
Si	2.58	0.04	5.63	0.07	2.66	0.12	2.67	0.03	2.73	0.03	2.78
^{IV}Al	1.42	0.04	2.37	0.07	1.34	0.12	1.33	0.03	1.27	0.03	1.22
^{VI}Al	1.34	0.03	2.13	0.15	0.56	0.11	0.46	0.04	0.61	0.05	0.54
Ti	0.01	0.01	0.03	0.02	0.07	0.03	0.17	0.04	0.11	0.02	0.13
Fe	3.14	0.04	4.42	0.30	1.35	0.00	1.40	0.06	1.33	0.04	1.27
Mn	0.04	0.01	0.02	0.01	0.01	0.37	0.00	0.00	0.01	0.0	0.01
Mg	1.49	0.03	2.19	0.18	1.07	0.01	0.79	0.09	0.84	0.01	0.75
Σ_{oct}	6.03	0.06	8.81	0.13	3.05	0.09	2.82	0.04	2.90	0.05	2.70
Ca	0.01	0.01	0.11	0.05	0.03	0.23	0.02	0.01	0.05	0.00	0.01
Na	0.02	0.01	0.03	0.05	0.08	0.01	0.02	0.01	0.03	0.00	0.12
K	0.01	0.01	0.30	0.16	0.38	0.04	0.82	0.04	0.55	0.07	0.24
NH_4			0.36		0.17						0.63
Σ_{int}	0.04	0.03	0.80	0.11	0.69	0.12	0.86	0.04	0.63	0.01	1.00
X_{Mg}	0.32	0.02	0.34	0.04	0.41	0.06	0.36	0.03	0.39	0.01	0.38
O	14		25		11		11		11		11

* Average estimate value for each sample.

the average K content in golden biotite is intermediate between that found in red biotite and the average suhailite composition determined by Ruiz Cruz and Sanz de Galdeano (2009a) (Table 5, analysis 6).

Selected chemical diagrams (Fig. 6) have been constructed using chlorite, mixed-layer, and vermiculite formulas calculated on the basis of 11 oxygen apfu to favor the comparison. In these plots, chlorite, mixed-layers, and vermiculite show uniform trends, revealing a negative correlation between Si and Fe+Mg (Fig. 6a) and a positive correlation between Si and Al/(Fe+Mg) (Fig. 6b), Si and Ca+Na+K (Fig. 6c), and Ti and Ca+Na+K (Fig. 6d) at the transition from typical chlorite to typical vermiculite. The plots also reveal that biotite (especially red biotite) shows slightly different trends in the Fe+Mg vs. Si plot and an inverse trend in the Ca+Na+K vs. Si plot. Maximum interlayer occupancy in biotite (0.906 apfu) has been measured in red biotite, whereas golden biotite shows a range of interlayer occupancies between 0.74 and 0.61 apfu. The average suhailite analysis taken from Ruiz Cruz and Sanz de Galdeano (2009a) is near the Si-richer golden biotite Figures 6a and 6b. The plots reveal, moreover, that phyllosilicates from samples BE-13, BE-12, and BE-4 define three fields, interpreted as corresponding to (1) chlorite, (2) mixed-layers, and (3) vermiculite.

Selected chemical data for white mica and other metamorphic phases are reported in Table 6. Most white mica from chlorite, vermiculite, and biotite schists shows Si contents between 3.04 and 3.10 apfu, Al contents > 2.7 apfu, Fe+Mg contents < 0.20 apfu, and interlayer occupancy on the order of 0.85 apfu, suggesting some illitic substitution. In contrast, white mica from sample BE-4 shows Si contents between 3.20 and 3.27 apfu, Al contents < 2.7 apfu, and Fe+Mg contents > 0.30 apfu (Table 6, analyses 1–4). Nevertheless, no textural differences between muscovite and phengite were observed, suggesting that white mica from sample BE-4, which is very fine grained, may be contaminated by intergrown vermiculite or Fe-oxide.

Plagioclase shows very uniform compositions within each sample and also throughout the sequence. Indeed only a slight decrease in An (from 32 to 23%) is observed at increasing metamorphic grade (Table 6, analyses 5–8).

We have obtained chemical profiles of garnet grains throughout the sequence (not reported here), but some representative analyses are shown in Table 6 (analyses 9–12). Sample BE-12 garnet shows very little zonation and has high grossular content. Garnet from sample BE-4 shows, in contrast, higher spessartine and lower grossularite contents. Garnet in sample BE-3 is present only as small inclusions within staurolite.

Chloritoid grains from chlorite and vermiculite schists (Table 6, analysis 13) are very homogeneous and characterized by low X_{Mg} (from 0.11 to 0.14). Staurolite grains from biotite schist are homogeneous (Table 6, analysis 14) with very low X_{Mg}.

TEM-AEM STUDY

The results of the TEM-AEM study of these samples are very similar to those described by Ruiz Cruz and Nieto (2006), although assemblages only consisting of chlorite or chlorite+mica:chlorite mixed-layers, corresponding to the beginning of the chlorite transformation, are not available in the samples selected for the present study. Importantly, sample BE-3 contains red biotite with almost complete interlayer occupancy, which had not been previously studied.

In sample BE-13, containing the assemblage chlorite+vermiculite according to the XRD patterns, the lattice-fringe images reveal that, in addition to chlorite and vermiculite packets, mixed-layer areas are also frequently associated with discrete chlorite packets (Fig. 7a). Vermiculite and chlorite exhibit both coherent and semi-coherent boundaries. Vermiculite

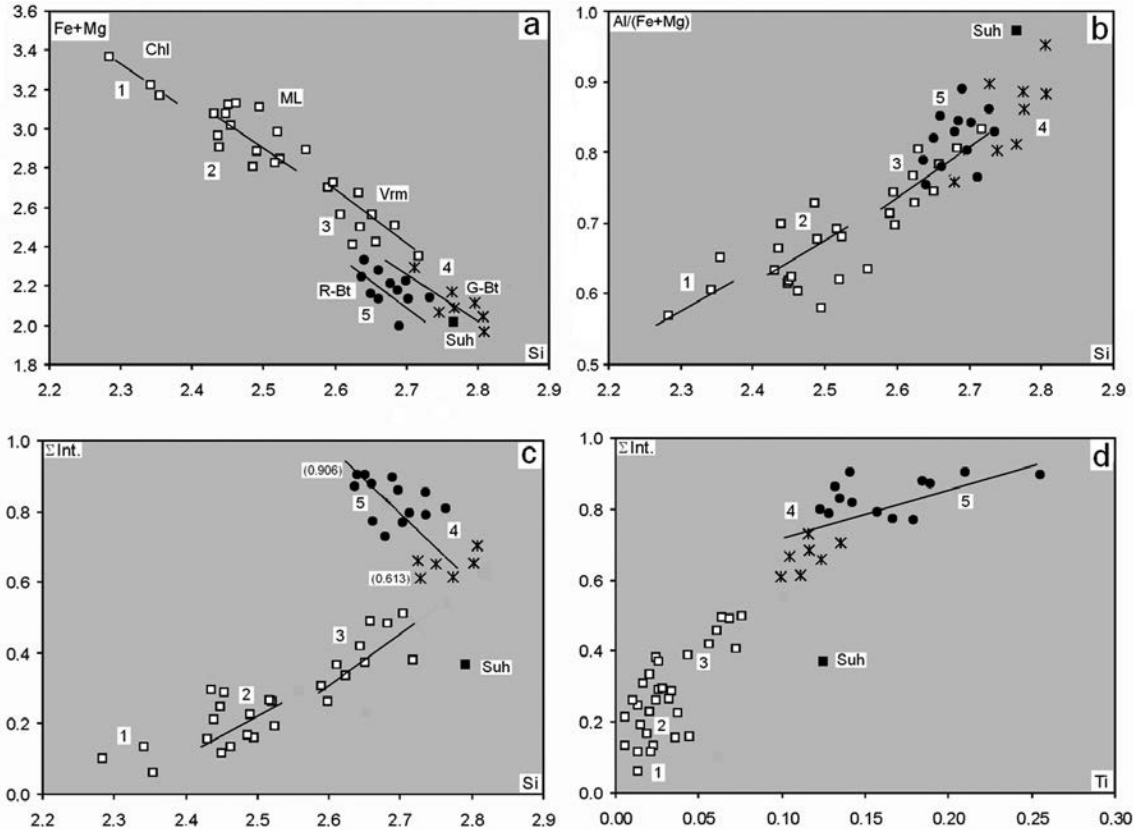

FIGURE 6. Chemical plots showing the most significant variations associated with the chlorite → mixed-layer chlorite-vermiculite → vermiculite transition (empty squares) in the Maláguide and Benamocarra samples. The compositions of golden and red biotite (sample BE-3), are represented by crosses and full circles, respectively. The five main populations (1, 2, 3, 4, and 5) correspond to chlorite, mixed-layer chlorite-vermiculite, vermiculite, golden biotite, and red biotite, respectively. The average composition for Suh (Ruiz Cruz and Sanz de Galdeano 2009a) has also been plotted (full square). In **c**, the numbers in parentheses indicate the maximum and minimum (Ca+Na+K) contents (apfu) in biotite.

TABLE 6. Selected chemical data for associated phases

	White mica					Plagioclase					Garnet					Cld	St
	BE-13	BE-12	BE-4	BE-3		BE-13	BE-12	BE-4	BE-3		BE-12(r)	BE-12(c)	BE-4(r)	BE-4(c)		BE-13	BE-3
	1	2	3	4		5	6	7	8		9	10	11	12		13	14
SiO_2	45.64	46.37	47.88	46.36		60.99	61.16	62.01	62.16		37.08	37.00	36.08	36.52		23.86	27.10
Al_2O_3	35.14	35.02	31.26	35.79		25.11	24.15	23.50	23.92		20.59	20.59	17.95	18.26		38.17	54.64
TiO_2	0.63	0.40	0.24	0.64		0.15	0.00	0.00	0.03		0.13	0.12	0.15	0.20		0.01	0.56
Cr_2O_3	0.29	0.03	0.15	0.03		0.03	0.00	0.03	0.00		0.01	0.00	0.19	0.24		0.10	0.02
FeO	1.84	2.25	4.07	0.81		0.00	0.00	0.10	0.00		32.24	32.76	35.30	33.83		27.96	13.97
MnO	0.01	0.00	0.12	0.00		0.00	0.16	0.00	0.00		0.58	0.61	6.95	6.59		0.91	0.26
MgO	0.53	0.85	1.27	0.39		0.09	0.01	0.00	0.00		1.94	1.82	1.43	1.29		1.96	0.95
CaO	0.02	0.08	0.21	0.03		6.27	5.97	5.24	5.23		7.41	7.07	1.96	3.12		0.00	0.01
Na_2O	0.53	0.48	0.00	0.50		7.14	8.21	8.54	8.57		0.01	0.00	0.00	0.00		0.01	0.01
K_2O	10.41	9.29	9.84	10.16		0.22	0.29	0.38	0.17		0.01	0.01	0.01	0.000		0.02	0.03
Total	95.04	95.05	95.05	95.04		99.98	99.96	99.85	100.25		99.99	99.98	100.03	100.06		92.99	97.72
Si	3.05	3.09	3.22	3.08	Si	2.68	2.72	2.76	2.75	Si	2.99	2.97	2.97	3.00	Si	2.01	3.78
^{IV}Al	0.96	0.91	0.78	0.91	Al	1.33	1.26	1.23	1.25	Al	1.95	1.94	1.74	1.77	Al	3.79	9.37
^{VI}Al	1.83	1.85	1.69	1.89	Ti	0.01	0.00	0.00	0.00	Ti	0.01	0.01	0.01	0.01	Fe^{3+}	0.21	
Ti	0.03	0.02	0.01	0.03	Fe	0.00	0.01	0.00	0.00	Cr	0.00	0.00	0.01	0.02	Ti	0.00	0.06
Cr	0.01	0.00	0.01	0.00	Mn	0.00	0.00	0.00	0.00	Fe^{3+}	0.06	0.10	0.28	0.20	Cr	0.01	0.00
Fe	0.10	0.13	0.23	0.04	Mg	0.01	0.00	0.00	0.00	Fe^{2+}	2.11	2.07	2.15	2.12	Fe^{2+}	1.76	1.63
Mn	0.00	0.00	0.01	0.00	Ca	0.33	0.28	0.25	0.25	Mn	0.04	0.04	0.49	0.46	Mn	0.07	0.03
Mg	0.05	0.09	0.12	0.04	Na	0.66	0.71	0.70	0.70	Mg	0.23	0.23	0.18	0.16	Mg	0.25	0.20
Σ_{oct}	2.02	2.07	2.05	2.01	K	0.01	0.02	0.02	0.01	Ca	0.61	0.65	0.17	0.27	X_{Mg}	0.11	0.11
Ca	0.00	0.01	0.02	0.00													
Na	0.07	0.06	0.00	0.07	An	33	28	25	25	Alm	71	70	73	71			
K	0.9	0.79	0.84	0.86	Ab	66	70	73	74	Prp	8	8	6	5			
Σ_{int}	0.96	0.86	0.86	0.92	Or	1	2	2	1	Grs	20	21	5	8			
										Sps	1	1	16	16			

exhibits 10 and 20 Å periodicities (corresponding to contracted 14 and 28 Å layers). Large, lens-shaped gaps formed during contraction against the electron beam were mainly formed between chlorite and vermiculite packets. Mixed-layers show sequences of 24 Å (corresponding to one chlorite + one contracted vermiculite layer) and sequences of 38 Å (corresponding to two chlorite + one contracted vermiculite layers, i.e., a chlorite:corrensite sequence). The SAED patterns show (except for chlorite), streaked basal reflections, reflecting an intimate mixture of the variety of structures described herein (Fig. 7a, inset).

Lattice-fringe images obtained from sample MP-12, which contains the assemblage chlorite:vermiculite mixed-layers+vermiculite, reveal poorly defined boundaries between these phases, with frequent transitions between them that occur parallel and oblique to the layers (Fig. 7b). Mixed-layer phases show a dominant 24 Å periodicity and vermiculite a 20 Å periodicity, suggesting the presence of a polytype with two layers.

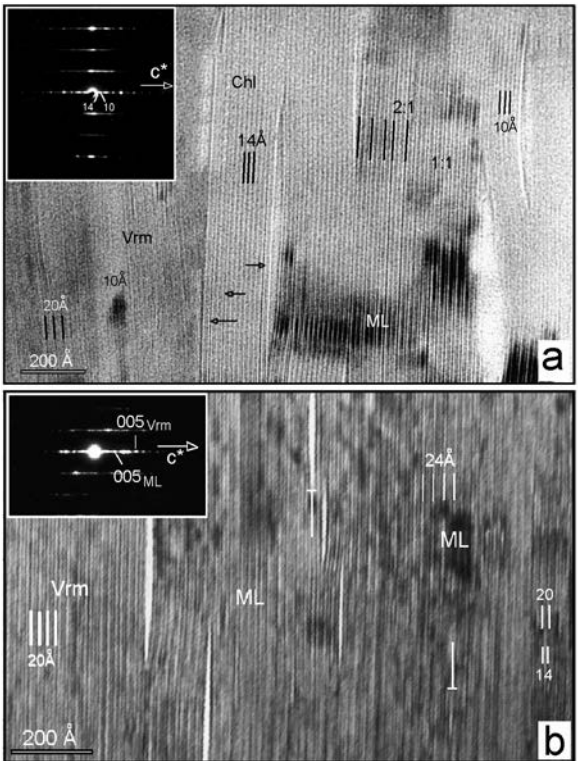

Figure 7. Representative TEM images of the trioctahedral phyllosilicate assemblages in samples BE-13 (**a**) and BE-12 (**b**). Although sample BE-13 has the assemblage Chl+Vrm according to the XRD patterns, areas containing 1:1 and 2:1 chlorite-vermiculite mixed-layers are associated with the chlorite packets (**a**). Large gaps due to vermiculite contraction against the electron beam mainly appear at the boundaries between chlorite and vermiculite (or mixed-layers). Arrows mark isolated vermiculite layers included in the chlorite packets. The SAED pattern (inset) shows streaking of the basal reflections, due to superposition of the reflections of several phases. Sample BE-12, with assemblage ML+Vrm mainly shows 1:1 sequences with 24 Å periodicity, corresponding to mixed-layers, and 20 Å sequences of vermiculite (**b**). Gaps due to layer contraction are thinner than in sample BE-13 and appear to be randomly distributed.

Gaps due to contraction are thin and appear randomly distributed in this sample. Reflections from the two phases can be identified in the SAED patterns (Fig. 7b, inset).

In sample BE-4, with dominant vermiculite, the lattice-fringe images are similar to those observed in sample BE-12, although mixed-layer areas are lacking (Fig. 8). Wavy layers and abundant layer terminations characterize the vermiculite packets (Fig. 8a). Indeed, careful determination of the basal periodicity indicates a range of values between ~10 and ~14 Å. The SAED patterns correspond to a two-layer polytype (Fig. 8a, inset), although they exhibit additional reflections corresponding to a 7 Å phase (suspected to be from kaolinite). The presence of two-layer sequences (Fig. 8b) is especially evident in some areas such as that shown in Figure 8c, where gaps isolate areas with 20 or 40 Å periodicity. Detailed examination (Fig. 8c, inset) suggests that the ~20 Å fringes appear to consist of two layers with slightly different thicknesses (~9 and ~10 Å).

Red biotite from sample BE-3 shows lattice fringe images characterized by thick packets with uniform 10 Å basal spacing (Fig. 9a) and numerous cleavage planes. Associated with some cleavage planes are thin packets (~50 Å) of retrograde kaolinite. The high-resolution images (Fig. 9a, inset) reveal uniform 10 Å periodicity and suggest the presence of the 1*M* polytype, as also indicated by the SAED patterns. Areas of golden biotite show thinner packets and less-ordered structures, including thin gaps due to contraction, and abundant layer-terminations associated with contrast effects (Fig. 9b). The SAED patterns also reveal abundant stacking disorder (Fig. 9b, inset). The presence of minor amounts of vermiculite (and biotite-vermiculite mixed-layers) could not be detected in the lattice-fringe images.

Discussion

A sequence of samples, including the complete pre-Permian Maláguide sequence and the upper Benamocarra terms was previously used by Ruiz Cruz and Nieto (2006) for illustrating the transition from chlorite to biotite during prograde metamorphism. These authors described samples containing vermiculite (sample N-5) and "low-charge" biotite (sample N-6). Although these results are valid in general, it is evident from the new data that the interlayer charge in vermiculite was underestimated because the presence of interlayer NH_4 was not accounted for, and that "low-charge biotite" (with interlayer charge ~0.65) actually corresponds to NH_4-bearing biotite. The significance of the presence of NH_4 in the transitional phases is discussed in the following sections.

Mineralogical and metamorphic evolution in the studied sequence

The rocks studied cover a wide metamorphic range, ranging from garnet-free samples to sillimanite-bearing samples. Garnet-free samples from the Maláguide complex are characterized by the presence of chlorite; garnet-rich samples from the Benamocarra unit are characterized by the prevalence of vermiculite (±chlorite:vermiculite mixed-layers); and typical sillimanite-andalusite-staurolite schists from the Alpujárride complex mainly contain biotite. Whereas the transition between the Maláguide and Benamocarra units seems to be gradual, a jump in metamorphic grade is observed between the Benamo-

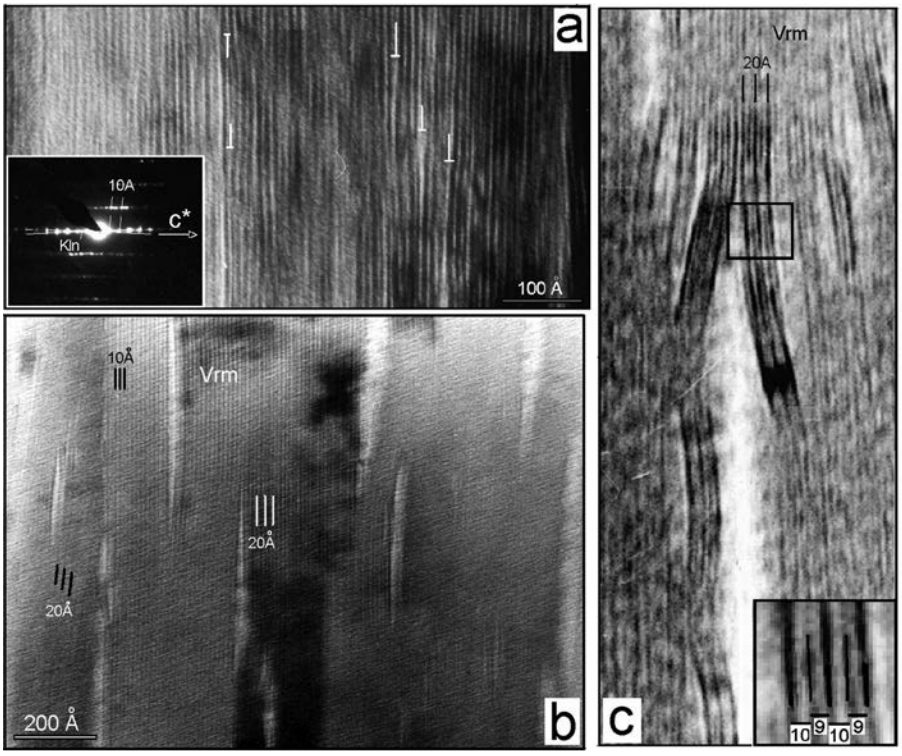

FIGURE 8. Lattice-fringe images from sample BE-4. (**a**) Vermiculite is characterized by wavy fringes (with basal periodicity between 10 and 14 Å) and abundant layer terminations. (**b**) Vermiculite shows uniform basal spacing, associated with numerous gaps. The 20 Å fringes shown in **c** appear to consist of two layers with slightly different basal spacing.

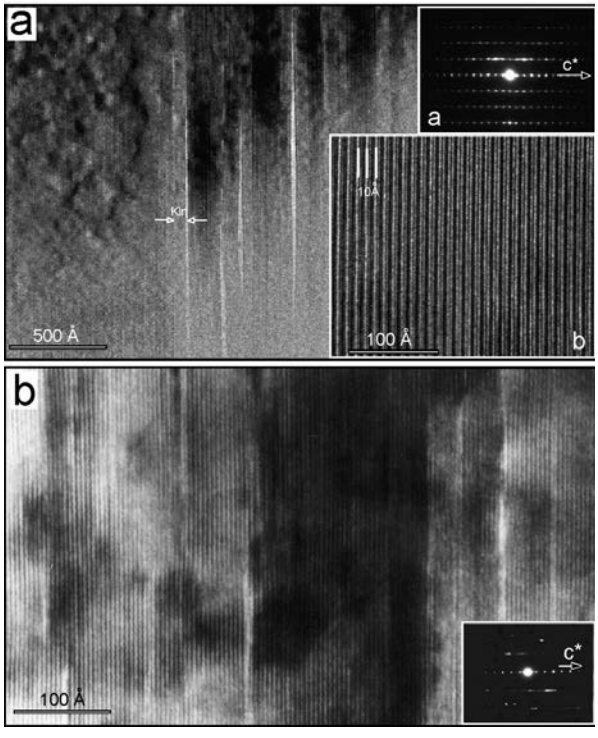

carra and the Alpujárride units. This jump is clearly reflected in the chemical plots shown in Figures 6c and 6d, in which biotite from sample BE-3 shows chemical trends different from the chlorite → vermiculite series observed in the overlying schists.

The nature of the transitional phases

Although the vermiculitic nature of the trioctahedral phases in the samples studied is unambiguously demonstrated from the XRD patterns obtained after different treatments and from the thermal behavior, the fact that the NH_4-bearing vermiculite and mixed-layers chlorite-vermiculite show a 14 Å spacing is intriguing. It is assumed that the NH_4 ion prefers to be in a dehydrated state, and the expected basal spacing would be in the 10.5–11.5 Å range for NH_4-saturated vermiculite.

The cause of the high basal spacing shown by our vermiculite is unknown but several considerations must be taken into account

(1) Previous investigations have demonstrated the influence of factors such as the magnitude of the interlayer surface charge, the location of the charge-deficiency sites, the total surface-

◄ **FIGURE 9.** Lattice-fringe image of biotite from sample BE-3. (**a**) Images of red biotite, showing the presence of abundant cleavage planes and thin packets of retrograde kaolinite. (Inset **a**) SAED pattern corresponding to the 1*M* polytype. (Inset **b**) A high-resolution image reveals the presence of an ordered 1-layer sequence. (**b**) Image of golden biotite. Contract effects are associated with layer terminations. The SAED pattern (inset) suggests the presence of stacking disorder.

charge density, the oxidation state of iron Fe, the nature of the bonds, the presence of an hydroxyl-interlayer, and the manner of packing of the water molecules, as being significant to the swelling properties, in addition to the cation composition, relative humidity, and temperature.

For example, vermiculite with higher layer charge (e.g., 0.8) will readily collapse, whereas vermiculite with lower layer charge (e.g., 0.6) will readily expand (Moore and Reynolds 1997). Also, the presence of an hydroxyl-interlayer will prop the structures open and the XRD characteristics will begin to resemble those of chlorite (Wang et al. 2011).

If the interlayer cation-to-layer bonds are considered as ideally electrostatic, the magnitude of the forces resisting expansion may be expressed as a form of Coulomb's law (Kerns and Mankin 1968). Nevertheless, in NH_4-vermiculite the NH_4^+ ion can establish several hydrogen bonds with oxygen atoms from the surface of the clay mineral layers and with water, which must necessarily influence the basal spacing.

Similarly, the oxidation state of iron Fe in the crystal structure of smectite and vermiculite profoundly alters their physical–chemical properties. Among the properties affected are layer charge, cation exchange and fixation capacity, swelling, layer stacking order and octahedral site occupancy. Also affected is the surface chemistry of the vermiculite, which alters the clay–water interaction mechanisms (Stucki et al. 2002).

Moreover, the extent of expansion, for a given number of monomolecular layers depends on the manner of packing of the water molecules. For example, Barshad (1949) concluded that it is not necessary to assume lattice layers with different degrees of hydration to explain certain variations in interlayer distances.

(2) The most common interlayer cation in natural vermiculite is magnesium. Although experiments leading to Na-, Ca-, K-NH_4-saturated vermiculites have been frequently realized in soils, the obtained results cannot be directly applied to natural phases. For example, Gruner (1939) showed that treatment of vermiculite with H_2O_2 directly produced a ~10 Å NH_4-mica. In contrast, basal spacing between 10.8 and 13 Å have been described for NH_4-exchanged vermiculites (MacEwan and Wilson 1980; Mamo et al. 1993). In all cases, NH_4 was in excess during the experiments, suggesting that these high basal spacings could really correspond to chlorite-NH_4-mica mixed-layers.

The available data for K-bearing natural vermiculite are very scarce and completely lacking for NH_4-vermiculite. Potassium-bearing natural vermiculite has been described as a product of the alteration of biotite and as a prograde phase intermediate between chlorite and biotite. In the first case, data about the chemical composition of the weathered biotite and the basal spacing of the natural samples are lacking in the most recent studies (see, for example, Murakami et al. 2003). Data reported by Ghabru et al. (1989) indicate, however, that vermiculite formed from biotite contains between 3 and 5 wt% of K_2O; i.e., the interlayer cation is mainly K, but the basal spacing of the samples is not reported. In the second case, it is evident that K-vermiculite is hydrated; indeed, the thermal behavior is similar to Mg-vermiculite (Black 1975; Velde 1978), although, according to Velde (1978), X-ray diffraction is not a positive identification method.

(3) Data such as the total surface-charge density, the oxidation state of iron Fe, the true nature of the bonds, and the manner of packing of the water molecules in our vermiculite are unknown. Indeed, it is also unknown how the NH_4^+ ion behaves in the presence of water. Whereas an approximately spherical shape is assumed in the case of NH_4-micas, it seems evident that, in the presence of water, the NH_4^+ ion must be as $NH_3 \cdot H_2O$ or $NH_4(OH)$, and that these molecules have a complex shape and dimensions notably higher than NH_4^+ (Fortes et al. 2001).

As a consequence, an accurate explanation of the 14 Å basal spacing of our K-NH_4-bearing vermiculite as well as of the relative intensities of the 001 and 002 reflections, which do not correspond to typical vermiculite, would require the determination of the interlayer structure. This type of determination, generally based on the position of the OH-stretching vibrations in the FTIR spectra (e.g., Bradley and Serratosa 1958), cannot be realized however, in samples containing several phyllosilicate populations. Simulations were realized using WINSTRUCT (Krumm 1999) and the composition of our vermiculite. Although not conclusive, the simulated patterns (Fig. 10) reveal that a notable increase of the I_{002}/I_{001} ratio is observed when we assume that the phase is a "pillared vermiculite", with a chlorite-like structure (Figs. 10a and 10b). A better fitting is obtained, however, assuming that both OH groups and water are present in the interlayer (Fig. 10c).

Influence of NH_4 on the mixed-layers and vermiculite XRD patterns

Drits et al. (1997) discussed the possible distribution of NH_4 in illite-smectite mixed-layers and the influence on the diffractions patterns. In the case of the mixed-layer and vermiculite structures described here, NH_4 distribution could be either homogeneous: i.e., all vermiculite (or mixed-layer) interlayers contain K and NH_4, or ordered: i.e., K-interlayers alternate with NH_4-interlayers. In both cases, the d_{001} values must increase proportionally to the content of NH_4, whereas the full-width at half height (FWHH) (00*l*) values should show different behaviors for these two interlayer cation distribution types. The evolution of the basal spacing of vermiculite from sample BE-13 to BE-4 indicates a slight increase (from 14.283 to 14.301 Å, Table 2) at increasing NH_4 contents in whole rock (from 0.061 to 0.082 wt%, Table 3) but does not permit an accurate estimation of the basal spacing for the final K- and NH_4-terms. Determination of the FWHH (00*l*) of selected reflections of vermiculite from sample BE-4 (not influenced by the presence of reflections of other phases), following a methodology similar to that described by Drits et al. (2005), indicates a slight decrease of FWHH at increasing *l*, suggesting that vermiculite shows a homogeneous distribution of NH_4 in all the interlayers. Although the lattice-fringe images (Fig. 8c) suggest an ordered distribution, this may occur only locally, whereas the data derived from the XRD patterns have probably a more general significance.

The role of mixed-layers and vermiculite in the chlorite-to-biotite reaction

Ruiz Cruz and Nieto (2006) claimed that the chlorite-to-biotite transition at increasing metamorphic grade is more

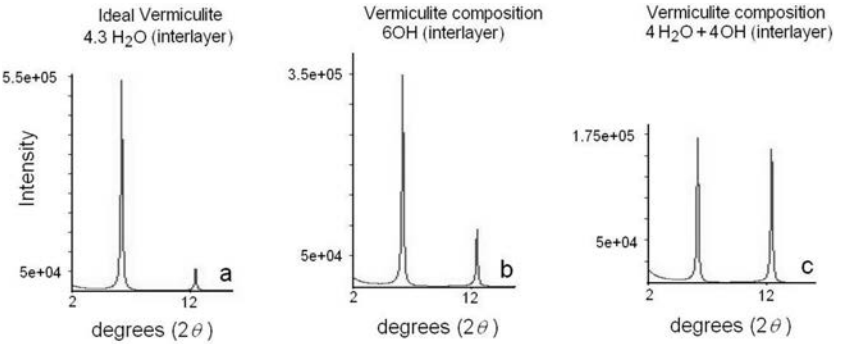

FIGURE 10. Simulated XRD patterns for vermiculite. (**a**) Ideal vermiculite structure, (**b**) chlorite structure, (**c**) pillared vermiculite structure. In all cases, the composition of our vermiculite has been used.

complex than previously assumed. The described sequence was: chlorite → ordered 1:2 mica–chlorite mixed-layers → ordered 1:1 chlorite–vermiculite mixed-layers → vermiculite → biotite. This sequence included a continuous increase of interlayer cation content.

In the dioctahedral series, which has been extensively studied (e.g., McCarty et al. 2009; Lanson et al. 2009, and references therein), the illitization process occurs through a wide series of mixed-layered structures, leading to micas with incomplete interlayer occupancy (illite and bramallite), and later to muscovite. There are also wide possibilities for intermediate phases between chlorite and biotite, and consequently the transition from chlorite to biotite throughout intermediate compositions could follow different pathways. Nevertheless, in the trioctahedral series, specially described in retrograde processes (Banfield and Eggleton 1988; Shau et al. 1990; Banfield and Murakami 1998), only ordered mixed-layers of the type corrensite or chlorite:corrensite have been described. In our case, the transitional phases include a 1:1 chlorite:vermiculite structure (and minor 1:1 chlorite:corrensite) and a vermiculite structure. Previous data (Ruiz Cruz 1999; Ruiz Cruz and Nieto 2006), as well as those presented here indicate that mixed-layer phases represent an earlier step in the transformation, whereas more advanced transformation leads to vermiculite.

The intermediate phases have been only rarely described in prograde sequences, where a direct transformation of chlorite into biotite is commonly assumed (Bucher and Frey 2002). This strongly suggests that the formation of intermediate phases can be favored in the presence of NH_4.

The role of NH_4 in the formation of intermediate phases

We interpret that NH_4 derived from organic matter maturation was initially contained in dioctahedral mica (NH_4-bearing illite) and was incorporated in the structure of the trioctahedral phases formed at increasing metamorphic grade, when illite becomes muscovite. Then, it seems that two coupled reactions must have taken place: the chlorite-to-vermiculite reaction and the NH_4-bearing illite-to-muscovite reaction. Many possibilities exist, but since the chlorite and vermiculite contents remain practically unchanged through the complete sequence (except in the biotite schist), and since the appearance of garnet, andalusite, and vermiculite are almost coincident, the coupled reaction could be:

$$1.1\text{Chl}+1.9\text{NH}_4\text{-illite}+7\text{Pl}(\text{An}_{33}\text{Ab}_{67})+2.2\ \text{Qz} \rightarrow 1\text{Vrm}+1\text{Ms}+2\text{Als}+1.25\text{Grt}+6.2\text{Pl}(\text{An}_{24}\text{Ab}_{76})+4.3\text{H}_2\text{O} \quad (1)$$

with chlorite formula from Table 5 (analysis 1), assumed NH_4-illite formula = $(NH_4K)_{0.9}(Al_{1.8}M^{2+}_{0.2})(Al_{0.7}Si_{3.3})O_{10}(OH)_2$, vermiculite formula from Table 5 (analysis 3), ideal muscovite and andalusite formulas, garnet formula from Table 6 (analysis 9), and plagioclase formulas from Table 6 (analyses 5 and 7).

In the dioctahedral series, in the presence of available NH_4, cation-deficient micaceous structures easily incorporate NH_4, thus favoring the illitization process. It is also known that most dioctahedral phases containing NH_4 have an illitic structure with low interlayer occupancy (Higashi 1982; Sterne et al. 1982; Daniels and Altaner 1990; Nieto 2002; Sucha et al. 2007). Juster et al. (1987) suggested that vacancies in the A site may result in weaker cohesion between layers and therefore to an expanded *c*-repeat distance.

It is also reasonable to assume that vacancies in the A site of a trioctahedral mica (cation deficient biotite) can result in weaker cohesion between layers, thus favoring the entry of NH_4 in these structures in relation with true biotite. And it seems also plausible that the cohesion between vermiculite and chlorite layers in the interstratified structure is weaker than between vermiculite layers, thus favoring the entry of NH_4 in these structures relative to vermiculite. All of these considerations suggest that the formation of transitional structures during the chlorite-to-biotite transformation can be favored in metasedimentary sequences initially rich in NH_4-illite, whereas direct transformation of chlorite into biotite would occur in the case of metasedimentary sequences containing typical K-illite.

CONCLUDING REMARKS

The NH_4 content and distribution in phyllosilicates has been investigated in metapelitic rocks ranging from the chlorite- to the sillimanite zone. The data presented here indicate that the NH_4 content in the studied samples is higher than in other metamorphic complexes and suggest that it depends on several factors, especially on the content and type of trioctahedral phyllosilicate. Maximum amounts of NH_4 are present in vermiculite from the transition between the chlorite and the garnet zones.

It is deduced that at higher metamorphic conditions than those characterizing the formation of NH_4-bearing dioctahedral

phases, the available NH_4 enters preferentially in transitional trioctahedral structures characterizing the chlorite-to-biotite transformation. By analogy to the dioctahedral smectite-to-illite transition, it seems reasonable to assume that alternation of layers with different structure and vacancies in the A site of a trioctahedral phase can result in weaker cohesion between layers, so favoring the entry of NH_4 in these structures, in relation to true biotite. In the case of the trioctahedral phases, both features (the presence of NH_4 and incomplete interlayer occupancy) appear to favor the hydration at superficial conditions leading to a ~14 Å basal spacing.

The presented data strongly suggest that the formation of transitional structures between chlorite and biotite, rarely described in metasedimentary sequences, is favored by the availability of NH_4, proceeding from the NH_4-bearing illite-to-muscovite transformation, in sequences initially rich in NH_4-illite.

Acknowledgments

The author is grateful to the Associate Editor W. Huff, to E.J. Daniels, and to an unknown reviewer, whose corrections and suggestions have notably improved the manuscript. To C. Sanz de Galdeano for help in fieldwork and for the discussion of the results; to M.M. Abad for help in obtaining TEM-AEM data; to M. Bentabol for the FTIR spectra; and to F. Franco and M.D. Rodríguez for mineral quantification from the XRD patterns. This study has received financial support from the Project CGL 2009-08186 (Ministerio de Ciencia e Innovación) and from the Research Group RNM-199 (Junta de Andalucía).

References cited

Azañón, J.M. and Goffé, B. (1997) Ferro- and magnesiocarpholite assemblages as record of high-P, low-T metamorphism in the Central Alpujárrides, Betic Cordillera (SE Spain). European Journal of Mineralogy, 9, 1035–1051.

Banfield, J.F. and Eggleton, R.A. (1988) Transmission electron microscope study of biotite weathering. Clays and Clay Minerals, 36, 47–60.

Banfield, J.F. and Murakami, T. (1998) Atomic-resolution transmission electron microscope evidence for the mechanism by which chlorite weathers to 1:1 semi-regular chlorite-vermiculite. American Mineralogist, 83, 348–357.

Barshad, I. (1949) The nature of lattice expansion and its relation to hydration in montmorillonite and vermiculite. American Mineralogist, 675–684.

Black, P.M. (1975) Mineralogy of New Caledonian metamorphic rocks. IV. Sheet silicates from Ouégoa district. Contributions to Mineralogy and Petrology, 49, 269–284.

Boyd, S.R. and Philippot, P. (1998) Precambrian ammonium biogeochemistry: a study of the Moine metasediments. Chemical Geology, 144, 257–268.

Bradley, W.F. and Serratosa, J.M. (1958) A discussion on the water content of vermiculite. Clays and Clay Minerals, 58, 260–270.

Brown, E.H. (1967) The greenschist facies in part of eastern Otago, New Zealand. Contributions to Mineralogy and Petrology, 14, 259–292.

Bucher, K. and Frey, M. (2002) Petrogenesis of Metamorphic Rocks, 341 p. Springer, Berlin.

Busigby, V., Cartigny, P., Philippot, P., and Javoy, M. (2003) Ammonium quantification in muscovite by infrared spectroscopy. Chemical Geology, 198, 21–31.

Cliff, G. and Lorimer, G.W. (1975) The quantitative analysis of thin specimens. Journal of Microscopy, 103, 203–207.

Chourabi, B. and Fripiat, J.J. (1981) Determination of tetrahedral substitution and interlayer surface heterogeneity from vibrational spectra of ammonium in smectites. Clays and Clay Minerals, 29, 260–268.

Daniels, E.J. and Altaner, S.P. (1990) Clay mineral authigenesis in coal and shale from the Anthracite region, Pennsylvania. American Mineralogist, 75, 825–839.

Drits, V.A., Lindgreen, H., and Salyn, A.L. (1997) Determination of the content and distribution of fixed ammonium in illite-smectite by X-ray diffraction: Application to North Sea illite-smectite. American Mineralogist, 82, 79–87.

Drits, V.A., Sakharov, B.A., Salyn, A.L., and Lindgreen, H. (2005) Determination of the content and distribution of fixed ammonium in illite-smectite using a modified X-ray diffraction technique: Application to oil source rocks of western Greenland. American Mineralogist, 90, 71–84.

Duit, W., Jansen, J.B.H., Van Breemen, A., and Boss, A. (1986) Ammonium micas in metamorphic rocks as exemplified by Dôme de l'Agot (France). American Journal of Science, 286, 702–732.

Elorza, J.J. and García-Dueñas, V. (1981) Mapa geológico y memoria de la hoja n° 1054, Velez-Málaga. Mapa Geológico de España 1:50.000. IGME, Madrid.

Estévez, C. and Chamón, C. (1972) Mapa geológico y memoria de la hoja n° 1053-1064, Málaga-Torremolinos. Mapa Geológico de España 1:50.000. IGME, Madrid.

Farmer, V.C. (1974) The layer silicates. In V.C. Farmer, Ed., The Infrared Spectra of Minerals, p. 331–365. Mineralogical Society, London.

Fortes, A.D., Brodholt, J.P., Wood, I.G., and Vocadlo, L. (2001) Ab initio simulation of ammonia monohydrate NH3.H2O and ammonium hydroxide NH4OH. Journal of Chemical Physics, 115, 7006–7014.

Franceschelli, M., Mellini, M., Memmi, I., and Ricci, C.A. (1986) Fine-scale chlorite–muscovite association in low-grade metapelites from Nurra (NW Sardinia), and the possible misidentification of metamorphic vermiculite. Contributions to Mineralogy and Petrology, 93, 137–143.

García-Casco, A. and Torres-Roldán, R. (1996) Disequilibrium induced by fast decompression in St–Bt–Grt–Ky–Sil–And metapelites from the Betic Belt (Southern Spain). Journal of Petrology, 37, 1207–1239.

Gautier, M., Mullera, F., L. Forestiera, L., Benya, J.-M., and Guegana, R. (2010) NH4-smectite: Characterization, hydration properties and hydro mechanical behaviour. Applied Clay Science, 49, 247–254.

Ghabru, S.K., Mermut, A.R., and Arnaud, R.J. (1989) Layer-charge and cation-exchange characteristics of vermiculite (weathered biotite) isolated from a gray luvisol in northeastern Saskatchewan. Clays and Clay Minerals, 37, 164–172.

Goffé, B., Michard, A., García-Dueñas, V., González-Lodeiro, F., Monié, P., Campos, J., Galindo-Zaldívar, J., Jabaloy, A., Martínez-Martínez, J.M., and Simancas, F. (1989) First evidence of high-pressure, low-temperature metamorphism in the Alpujarride nappes, Betic Cordillera (SE Spain). European Journal of Mineralogy, 1, 139–142.

Gruner, J.W. (1939) Ammonium mica synthesized from vermiculite. American Mineralogist, 24, 425–433.

Higashi, S. (1982) Tobelite, a new ammonium dioctahedral mica. Mineralogical Journal, 11, 138–146.

Honma, H. and Itihara, Y. (1981) Distribution of ammonium in minerals of metamorphic and granitic rocks. Geochimica et Cosmochimica Acta, 45, 983–988.

Johnson, L.J. (1964) Occurrence of regularly interstratified chlorite–vermiculite as a weathering product of chlorite in a soil. American Mineralogist, 49, 556–572.

Juster, T.C., Brown, P.E., and Bailey, S.W. (1987) NH_4-bearing illite in very low grade metamorphic rocks associated with coal, northeastern Pennsylvania. American Mineralogist, 72, 555–565.

Kerns, R.L. Jr. and Mankin, C.J. (1968) Structural charge site influence on the interlayer hydration of expandable three-sheets clay minerals. Clays and Clay Minerals, 16, 73–81.

Kerrick, D.M. and Cotton, W.R. (1971) Stability reactions of jadeite pyroxene in Franciscan metagreywackes near San José, California. American Journal of Science, 271, 350–369.

Krumm, S. (1999) Simulation of XRD patterns from oriented clay minerals with WinStruct. Computers & Geoscience, 25, 501–509.

Lanson, B., Sakharov, B.A., Claret, F., and Drits, V.A. (2009) Diagenetic smectite-to-illite transition in clay-rich sediments: A reappraisal of X-ray diffraction results using the multi-specimen method. American Journal of Science, 309, 476–516.

MacEwan, D.M.C. and Wilson, M.J. (1980) Interlayer and intercalation complexes of clay minerals. In G.W. Brindley and G. Brown, Eds., Crystal Structures of Clay Minerals and their X-ray Identification, p. 197–248. Mineralogical Society, London.

Mamo, M., Taylor, R.W., and Shuford, J.W. (1993) Ammonium Fixation by Soil and Pure Clay Minerals. Communications in Soil Science and Plant Analysis, 24, 1115–1126.

McCarty, D.K., Sakharov, B.A., and Drits, V.A. (2009) New insights into smectite illitization: A zoned K-bentonite revisited. American Mineralogist, 94, 1653–1671.

Maresch, W.V., Massone, H.-J., and Czank, M. (1985) Ordered and disordered chlorite/biotite interstratifications as alteration products of chlorite. Neues Jahrbuch für Mineralogie Abandlungen, 152, 79–100.

Mellini, M., Nieto, F., Alvarez, F., and Gómez-Pugnaire, M.T. (1991) Mica–chlorite intermixing and altered chlorite from the Nevado–Filábride micaschists. Southern Spain. European Journal of Mineralogy, 3, 27–38.

Moore, D. and Reynolds, R.C. Jr. (1997) X-Ray Diffraction and the Identification and Analysis of Clay Minerals, 2nd ed., 373 p. Oxford University Press, New York.

Murakami, T., Utsunomiya, S., Yokoyama, T., and Kasama, T. (2003) Biotite dissolution processes and mechanisms in the laboratory and in nature: Early stage weathering environment and vermiculitization. American Mineralogist, 88, 377–386.

Nicot, E. (1981) Les phyllosilicates des terrains précambriens du Nord–Ouest du Montana (USA) dans la transition anchizone-épizone. Bulletin de Minéralogie, 104, 615–624.

Nieto, F. (2002) Characterization of coexisting NH_4- and K-micas in very low-grade metapelites. American Mineralogist, 87, 205–216.

Proust, D. (1982) Supergene alteration of metamorphic chlorite in an amphibolite from Massif Central, France. Clay Minerals, 17, 159–173.

Proust, D., Eymery, J.P., and Beaufort, D. (1986) Supergene vermiculitization of a magnesian chlorite: iron and magnesium removal process. Clays and Clay

Minerals, 34, 572–580.
Ruiz Cruz, M.D. (1999) New data for metamorphic vermiculite. European Journal of Mineralogy, 11, 533–548.
——— (2001) Mixed-layers mica-chlorite in very low-grade metaclastites from the Maláguide Complex (Betic Cordilleras, Spain). Clay Minerals, 36, 307–324.
Ruiz Cruz, M.D. and Nieto, J.M. (2006) Chemical and structural evolution of "metamorphic vermiculite" in metaclastic rocks of the Betic Cordillera, Málaga, Spain: A synthesis. Canadian Mineralogist, 44, 249–265.
Ruiz Cruz, M.D. and Rodríguez Jiménez, P. (2002) Correlation between crystallochemical parameters of phyllosilicates and mineral facies in very low-grade metasediments of the Betic Cordillera (Spain): A synthesis. Clay Minerals, 37, 169–185.
Ruiz Cruz, M.D. and Sanz de Galdeano, C. (2008) High-temperature ammonium white mica from the Betic Cordillera (Spain). American Mineralogist, 93, 977–987.
——— (2009a) Suhailite: A new ammonium trioctahedral mica. American Mineralogist, 94, 210–221.
——— (2009b) Exsolution microstructures in NH4-bearing muscovite and annite in gneisses from the Torrox area, Betic Cordillera, Spain. Canadian Mineralogist, 47, 107–128.
——— (2010) Factors controlling the evolution of mineral assemblages and illite crystallinity in Paleozoic to Triassic sequences from the transition between Maláguide and Alpujárride complexes (Betic Cordillera, Spain): The significance of tobelite. Clays and Clay Minerals, 58, 558–572.
Russell, J.D. and White, J.L. (1988) Infrared study of the thermal decomposition of ammonium rectorite. Clays and Clay Minerals, 14, 181–191.
Sanz de Galdeano, C., Andreo, B., García-Tortosa, F.J., and López-Garrido, A.C. (2001) The Triassic palaeogeographic transition between the Alpujárride and Maláguide complexes. Betic-Rif Internal Zone. Palaeo, 167, 157–173.
Schroeder, P.A. and Ingall, E.D. (1994) A method for the determination of nitrogen in clays, with application to the burial diagenesis of shales. Journal of Sedimentary Research, A, 64, 694–697.
Shau, Y-H., Peacor, D.R., and Essene, E.J. (1990) Corrensite and mixed-layer chlorite/corrensite in metabasalt from northern Taiwan: TEM/AEM, EMPA, XRD, and optical studies. Contributions to Mineralogy and Petrology, 105, 123–142.
Sterne, E.J., Reynolds, R.C. Jr., and Zantop, H. (1982) Natural ammonium illites from black shales hosting a stratiform base metal deposit, Delong Mountains, northem Alaska. Clays and Clay Minerals, 30, 161–166.
Stucki, J.W., Lee, K., Zhang, L., and Larson, R.A. (2002) Effects of iron oxidation state on the surface and structural properties of smectites. Pure Applied Chemistry, 74, 2145–2158.
Sucha, V., Uhlik, P., Madejova, J., Petit, S., Kraus, I., and Puskelova, L. (2007) Particle properties of hydrothermal ammonium-bearing illite-smectite. Clays and Clay Minerals, 55, 36–44.
Tubía, J.M., Cuevas, J., Navarro-Vilá, F., Alvarez, F., and Aldaya, F. (1992) Tectonic evolution of the Alpujarride Complex (Betic Cordillera, southern Spain). Journal of Structural Geology, 14, 193–203.
Velde, B. (1978) High temperature or metamorphic vermiculites. Contributions to Mineralogy and Petrology, 66, 319–323.
Wang, C.F, Gu, H.Z., and Zhou, F. (2011) Investigation of inorganic-intercalated vermiculite by X-ray diffraction. Advanced Material Research, 177, 602–605.
Whitney, D.L. and Evans, B.W. (2010) Abbreviations for names of rock-forming minerals. American Mineralogist, 95, 185–187.
Zeck, H.P. and Williams, I.S. (2001) Hercynian Metamorphism in Nappe Core Complexes of the Alpine Betic-Rif Belt, Western Mediterranean-a SHRIMP Zircon Study. Journal of Petrology, 42, 1373–1385.

Manuscript received February 3, 2011
Manuscript accepted June 24, 2011
Manuscript handled by Warren Huff